Research Square

Preprints are preliminary reports that have not undergone peer review.
They should not be considered conclusive, used to inform clinical practice,
or referenced by the media as validated information.

Deformation Due to a Pair of Infinite and a Pair of infinite-finite planar faults in Fractional Standard Linear Solid

Pabita Mahato

pabitamahato012@gmail.com

National Institute of Technology Durgapur

Seema Sarkar (Mondal)

National Institute of Technology Durgapur

Debabrata Mondal

Sitananda College Nandigram

Research Article

Keywords: Interacting faults, Fractional Standard linear solid, Mittag-Leffer function, Green's function technique

Posted Date: June 24th, 2026

DOI: https://doi.org/10.21203/rs.3.rs-10064111/v1

License: This work is licensed under a Creative Commons Attribution 4.0 International License.
Read Full License

Additional Declarations: No competing interests reported.

Deformation Due to a Pair of Infinite and a Pair of infinite-finite planar faults in Fractional Standard Linear Solid

Pabita Mahato[1, 2*], Seema Sarkar (Mondal)[1†] and Debabrata Mondal[3†]

[1*]Department of Mathematics, National Institute of Technology Durgapur, Durgapur, 7713209, West Bengal, India.
[2]Department of Mathematics and Statistics, Amity School of Applied Sciences, Amity University, Mumbai, 410206, Maharashtra, India.
[3]Department of Mathematics, Sitananda College Nandigram, Nandigram, 721631, West Bengal, India.

*Corresponding author(s). E-mail(s): pabitamahato012@gmail.com, https://orcid.org/0000-0002-6859-2140;
Contributing authors: ssarkarmondal.maths@nitdgp.ac.in; debu.math34@gmail.com;
†These authors contributed equally to this work.

Abstract

It is frequently observed that seismically active regions contain multiple faults, and slip along one fault can significantly influence stress accumulation and distribution in the vicinity of neighboring faults. In our proposed work, we have considered two mathematical models, each involving two interacting planar faults; one model depicts the interaction between two infinite buried faults, and the other represents the interaction between an infinite buried fault and a finite surface-breaking fault. All faults exhibit strike-slip motion, creeping, and are located within a viscoelastic half-space of the fractional standard linear solid medium. The solution for displacement, stress, and strain components is found using the technique of fractional calculus when both faults move. Our derivation includes the Laplace transformation, modified Green's function technique, and the Correspondence principle. The accumulation of stress in the adjacent fault is analyzed due to the movement across the other fault. The effect that one creeping fault

has on another becomes stronger with increasing values of the order of the fractional derivative. These findings can enhance our understanding of subsurface deformation and its role in influencing fault dynamics and earthquake generation.

Keywords: Interacting faults, Fractional Standard linear solid, Mittag-Leffler function, Green's function technique

1 Introduction

In the study of earthquake mechanics, it is frequently observed that multiple faults coexist, especially in seismically active zones (e.g. Calaveras, San Jacinto, San Andreas, etc., are interacting faults). During the aseismic period, these faults often influence each other's behavior through stress transfer and deformation. Faults can be categorized based on their geometry and behavior. A fault is considered infinite if its length greatly exceeds its width; otherwise, it is termed finite. Based on the direction of slip, faults are classified as strike-slip when movement occurs parallel to the fault's strike, and dip-slip when the movement follows the dip direction. Additionally, faults can be grouped by the nature of their motion. Creeping faults exhibit slow, continuous displacement due to tectonic forces-typically on the order of cm per year, such as 2 cm/year. In contrast, locked faults remain stationary over time but may abruptly release accumulated stress through sudden slip events, often resulting in earthquakes.

Dynamic models of fault systems can involve either a pair of interacting strike-slip faults or a mix of dip-slip and strike-slip faults, reflecting the complex nature of fault interactions in seismically active regions. Maji et al. (1979) analyzed a system of two parallel, locked strike-slip faults and demonstrated that without any fault displacement, shear stress would steadily build up near the faults, eventually triggering a sudden slip on one of them and causing an earthquake. Later, Ghosh and others (1992) examined vertically interacting strike-slip faults and found that under certain conditions, aseismic slip on one fault can lead to the aseismic release of shear stress in the vicinity of both faults. Kato & Lei (2001) investigated how two parallel strike-slip faults interact within a layered geological medium. Their analysis highlighted the significance of structural layering in fault behavior. In a separate study, Parsons et al. (2003) demonstrated that earthquake ruptures are capable of jumping across fault gaps as wide as 4 km., although such rupture transfer likely requires specific stress conditions to occur. Additionally, Harris & Day (1993), using a two-dimensional finite difference modeling approach, explored how dynamic ruptures behave in the presence of fault steps. Their results showed that rupture fronts can traverse both compressional and dilational steps, with the potential to cross even relatively wide step-overs under favorable conditions.

Debnath and Sen (2014) derived analytical formulas to describe the displacements, stresses, and strains associated with two infinitely long interacting faults. Manna and Sen (2017) explored a theoretical framework involving interacting strike-slip faults

within a viscoelastic layered medium. More recently, Shao and Hou (2019) developed four sets of conceptual models to analyze how seismogenic faults respond to stress fields and contribute to earthquake activity. Additionally, Kundu and Sarkar (Mondal) (2020) examined the interaction between finite and infinite faults in a Maxwell-type viscoelastic half-space. All these models are integer models, i.e., they have used integer order derivative to solve the mathematical model.

However, it has been observed that fractional calculus is very much appropriate for describing memory of materials, which is often overlooked in traditional integer models. Several researchers are showing interest in fractional derivatives for modelling in different areas including viscoelastic systems, dielectric polarization (Podlubny 1999), robotics (Özalp & Demirci 2011), biological systems (Hilfer 2000), etc. Pelap et al. (2018) examined the influence of fractional-order derivatives within the framework of the Burridge-Knopoff 'train model' and demonstrated that the magnitude of earthquakes is significantly affected by the value of the fractional order. Analytical expressions of displacement, stresses, and strains for a long strike-slip fault in a fractional order Maxwell-type viscoelastic half-space are studied by Mondal and Debnath (2021). Very recently, an infinite strike-slip fault in a fractional standard linear solid was analyzed by Mahato et al. (2022) using fractional order derivatives. Kundu (2024) examined how ground deformation is influenced by the movement of a system of interacting faults, focusing on the interaction between a finite fault and a series of infinitely long faults.

In geophysical modeling, the lithosphere-asthenosphere system is frequently idealized as a viscoelastic half-space. This approach offers a balanced and practical framework for analyzing the mechanical response of Earth's outer layers. By simplifying the complex structure of the Earth into a viscoelastic continuum, researchers can effectively investigate the interplay between elastic and viscous deformation mechanisms that govern tectonic activities, such as plate motion, earthquake cycles, and post-seismic deformation. To capture these behaviors, the standard linear solid model is often employed. This model combines the essential characteristics of both Maxwell and Kelvin-Voigt elements, enabling it to simulate the immediate elastic response as well as the delayed viscous flow observed in real Earth materials (Segall, 2010).

In viscoelastic materials, the current state of stress and strain within a material is not solely determined by present forces but is also significantly influenced by the entire history of applied stresses and deformations. This intrinsic memory effect can be mathematically captured using time integrals, naturally leading to the framework of fractional calculus. Fractional derivatives are particularly well-suited for modeling viscoelastic behavior because they inherently incorporate these memory-dependent effects (Samko et al., 1993). Incorporating fractional derivatives into the constitutive relations of viscoelastic media, it becomes possible to more accurately represent the complex, time-dependent relationship between stress and strain (Deng and Morozov, 2018; Wu et al., 2023).

With these considerations, we have developed theoretical models to investigate ground deformation in the time of aseismic period in regions prone to seismic activity. Specifically, we examine two scenarios: (i) the interaction between two infinite buried faults, and (ii) the interaction between one infinite buried fault and a finite surface-breaking fault. The Earth's medium is modeled as a viscoelastic half-space representing the lithosphere-asthenosphere system, characterized by a fractional standard linear solid. This approach incorporates nonlinearity and long-term memory effects, offering a more realistic and comprehensive representation of the system's rheological behavior.

The remaining manuscript is organized as follows: In § 2, we comprehensively explain the models and formulas used for both cases. We then proceed to determine the solutions before and after the movement of the fault in § 3. In § 4, we present graphical representations of the numerical results and analyze them thoroughly. We conclude our findings and discuss the future directions of our work in § 5 and § 6, respectively. Finally, we added a "Declaration" statement and provided a list of references at the end.

2 Modelling of the problem

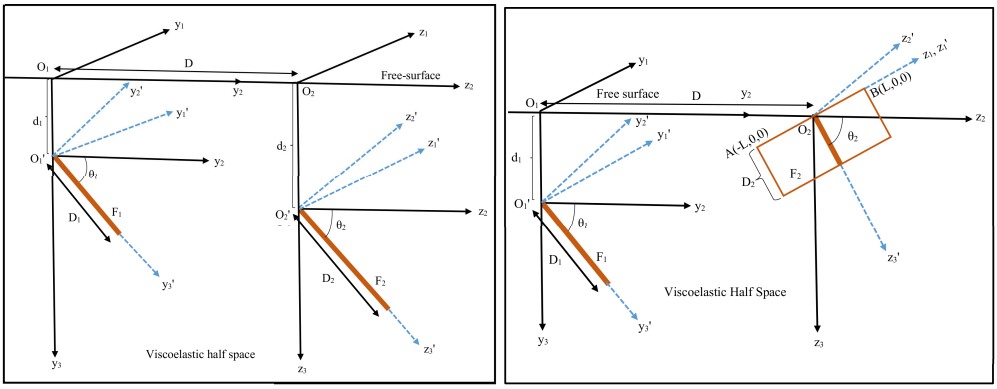
This study presents theoretical models involving two interacting inclined planar creeping strike-slip faults, denoted as F_1 and F_2, embedded within a viscoelastic half-space characterized by a fractional standard linear solid. The faults have respective widths D_1 and D_2, and are inclined at angles θ_1 and θ_2 to the free surface. The horizontal separation between the upper edges of the two faults is D. Two different cases have been studied by considering different types of interacting faults.
Case-I. Both F_1 and F_2 are infinite buried.
Case-II. The fault F_1 is infinite and buried while fault F_2 is finite and surface-breaking.

For case-I, let faults F_1 and F_2 be situated at a depth d_1 and d_2, respectively, below the free surface, and for case-II, let fault F_1 be located at a depth d_1 below the free surface while fault F_2 is surface breaking having a finite length of $2L$. Figure 1 below shows the schematic diagram of both models.

2.1 Mathematical formulation

To clearly define the positions of the faults, first we consider two rectangular Cartesian coordinate systems: (y_1, y_2, y_3) for fault F_1 and (z_1, z_2, z_3) for fault F_2. In both systems, the y_3 and z_3 axes point vertically downward, with $y_3 = 0$ representing the Earth's free surface. The y_1 and z_1 axes lie along the strike direction of the respective faults on the surface, while the y_2 and z_2 axes are normal to the y_1y_3 and z_1z_3 planes, respectively.

Additionally, we define two more coordinate systems: (y_1', y_2', y_3') for fault F_1 and (z_1', z_2', z_3') for fault F_2. In the system (y_1', y_2', y_3'), the y_3' axis runs along the width of fault F_1, the y_2' axis is normal to the fault plane, and the y_1' axis aligns with y_1, lying perpendicular to the $y_2'y_3'$ plane. Likewise, in the (z_1', z_2', z_3') system, the z_3' axis follows the width of fault F_2, the z_2' axis is perpendicular to its plane, and the z_1' axis



(a) (b)

Fig. 1: Schematic representation of the fault model (a) a pair of infinite buried faults and (b) an infinite buried fault coupled with a finite surface-breaking fault

is parallel to z_1, also perpendicular to the $z_2'z_3'$ plane. For case-I, the relation among the coordinate axes is given as

$$\begin{cases} y_1' = y_1 \\ y_2' = y_2 \sin\theta_1 - (y_3 - d_1)\cos\theta_1 \\ y_3' = y_2 \cos\theta_1 + (y_3 - d_1)\sin\theta_1 \end{cases} \qquad \begin{cases} z_1' = z_1 \\ z_2' = z_2 \sin\theta_2 - (z_3 - d_2)\cos\theta_2 \\ z_3' = z_2 \cos\theta_2 + (z_3 - d_2)\sin\theta_2 \end{cases} \tag{1}$$

such that

$$z_2 = y_2 - D, \qquad z_3 = y_3 \tag{2}$$

and for case-II, the relations among coordinate systems are

$$\begin{cases} y_1' = y_1 \\ y_2' = y_2 \sin\theta_1 - (y_3 - d_1)\cos\theta_1 \\ y_3' = y_2 \cos\theta_1 + (y_3 - d_1)\sin\theta_1 \end{cases} \qquad \begin{cases} z_1' = z_1 \\ z_2' = z_2 \sin\theta_2 - z_3 \cos\theta_2 \\ z_3' = z_2 \cos\theta_2 + z_3 \sin\theta_2 \end{cases} \tag{3}$$

such that

$$z_2 = y_2 - D, \qquad z_3 = y_3 \tag{4}$$

In Case I, the faults are assumed to be infinite, meaning their lengths are substantially greater than their widths. To simplify the analysis, a cross-sectional view is taken along the plane $y_1 = 0$. Within this section, the faults are represented as: $F_1 : y_2' = 0, 0 \leq y_3' \leq D_1$; $F_2 : z_2' = 0, 0 \leq z_3' \leq D_2$. In Case II, fault F_1 remains infinite, but fault F_2 is of finite length $2L$. Accordingly, the faults are defined as:

$F_1 : y_2' = 0,\ 0 \le y_3' \le D_1;\ F_2 : -L \le z_1' \le L,\ z_2' = 0,\ 0 \le z_3' \le D_2.$

Let u_1, u_2, u_3 be displacement components along y_1, y_2, y_3 respectively, τ_{11}, τ_{12}, $\tau_{13}, \tau_{22}, \tau_{23}, \tau_{33}$ be stress components and $e_{11}, e_{12}, e_{13}, e_{22}, e_{23}, e_{33}$ be strain components. Then the displacement, stress, and strain components for infinite strike-slip faults be $(u_1, \tau_{12}, \tau_{13}, e_{12}, e_{13})$ and that for finite fault be $(u_1, u_2, u_3, \tau_{11}, \tau_{12}, \tau_{13}, \tau_{22}, \tau_{23}, \tau_{33}, e_{11}, e_{12}, e_{13}, e_{22}, e_{23}, e_{33})$ (Mukhopadhyay (1980).

The analysis begins by considering an initial state in which no active fault motion is observed inside the medium. This time is considered as $t = 0$. The whole viscoelastic region is assumed to be in a quasi-static, aseismic condition, characterized by extremely slow, continuous deformation in the absence of seismic activity. In this context, "quasi-static" refers to a system where inertial effects are negligible, and all physical changes occur gradually over time.

Despite the lack of dynamic fault slip, the medium is subjected to persistent shear stresses, indicative of potential strike-slip motion. These stresses arise from long-term tectonic forces, including mantle convection, internal earth pressures, and other geophysical processes. Under these conditions, the displacement, stress, and strain components will satisfy some constitutive equation, stress equation of motion and boundary conditions, which govern the behaviour of the medium for time $t \ge 0$. These relationships are detailed in the following sections.

2.2 Case-I: Both F_1 and F_2 are infinite

2.2.1 Constitutive equations:

The stress-strain relations, also known as constitutive equations (Debnath, 2003), for the viscoelastic half-space of fractional order standard linear solid during the aseismic state for both the faults F_1 and F_2, are

$$\tau_{1j} + \frac{\eta}{\mu}\, {}_0D_t^{\alpha}\left(\tau_{1j}\right) = \mu \frac{\partial u_1}{\partial y_j} + 2\eta\, {}_0D_t^{\alpha}\left(\frac{\partial u_1}{\partial y_j}\right);\ j = 2, 3 \tag{5}$$

for $-\infty < y_2 < \infty, y_3 \ge 0,\ t \ge 0$.
where η denotes the effective viscosity while μ denotes the effective rigidity of the viscoelastic medium, ${}_0D_t^{\alpha}$ is Caputo fractional operator defined over the interval $[0, t]$ such that the range of the order α is $\alpha \in (0, 1]$, which is defined as

$${}_0D_t^{\alpha}(f(t)) = \frac{1}{\Gamma(1-\alpha)} \int_0^t \frac{f'(\xi)d\xi}{(t-\xi)^{\alpha}} \tag{6}$$

2.2.2 Stress equation of motion:

Assuming quasi-static deformation, where inertial forces are minimal and can be ignored, and body forces remain constant, the stress equation governing the system is

expressed as follows

$$\frac{\partial}{\partial y_2}(\tau_{12}) + \frac{\partial}{\partial y_3}(\tau_{13}) = 0 \tag{7}$$

where $-\infty < y_2 < \infty, y_3 \geq 0$ and $t \geq 0$.

2.2.3 Boundary Conditions:

In this scenario, we assume that fault F_1 moves prior to fault F_2. Therefore, the boundary conditions are formulated for the fault F_1 as follows.

We consider the tectonic force $\tau_\infty(t)$ that acts far away from the fault inside the lithosphere-asthenosphere system, increases slowly with time and is defined as $\tau_\infty(t) = \tau_\infty(0)(1 + kt)$, i.e.,

$$\tau_{12} \to \tau_\infty(0)(1 + kt) \text{ as } |y_2| \to \infty, \text{ for } y_3 \geq 0, t \geq 0 \tag{8}$$

such that k is a small positive constant, $\tau_\infty(0)$ denotes tectonic force at $t = 0$.
Stress τ_{13} decays with depth and becomes negligible in the far field, i.e.,

$$\tau_{13} \to 0 \text{ as } y_3 \to \infty \text{ for } -\infty < y_2 < \infty, t \geq 0 \tag{9}$$

and stress τ_{13} vanishes on the Earth surface i.e.,

$$\tau_{13} = 0 \text{ at } y_3 = 0 \text{ for } -\infty < y_2 < \infty \tag{10}$$

2.2.4 Initial conditions:

We start our observations at an instant of time $t = 0$ when no fault movement occurs across the faults and an aseismic state occurs. The values of $u_1, \tau_{12}, \tau_{13}, e_{12}, e_{13}$ at that instant are taken as $(u_1)_0, (\tau_{12})_0, (\tau_{13})_0, (e_{12})_0, (e_{13})_0$ respectively. All these initial values are constants or functions of y_2, y_3 only and satisfy all the relations (5), (7) to (10).

2.3 Case-II: F_1 is infinite and F_2 finite

2.3.1 Constitutive equations:

The constitutive equations for the infinite fault F_1 are taken as

$$\tau_{1j} + \frac{\eta}{\mu}\, {}_0D_t^\alpha\, (\tau_{1j}) = \mu \frac{\partial u_1}{\partial y_j} + 2\eta\, {}_0D_t^\alpha \left(\frac{\partial u_1}{\partial y_j}\right); j = 2, 3 \tag{11}$$

for $-\infty < y_2 < \infty, y_3 \geq 0$, $t \geq 0$,

and the constitutive equations for finite strike-slip fault F_2 are given as

$$\tau_{ij} + \frac{\eta}{\mu}\,{}_0D_t^{\alpha}\left(\tau_{ij}\right) = \frac{\mu}{2}\left(\frac{\partial u_i}{\partial y_j} + \frac{\partial u_j}{\partial y_i}\right) + \eta\,{}_0D_t^{\alpha}\left(\frac{\partial u_i}{\partial y_j} + \frac{\partial u_j}{\partial y_i}\right);\ i,j = 1,2,3 \quad (12)$$

for $-\infty < y_2 < \infty, y_3 \geq 0,\ t \geq 0$.

where $\tau_{ij} = \tau_{ji}$ for $i = j$ as we have considered a homogeneous isotropic medium, η and μ are the effective viscosity and effective rigidity of the viscoelastic half-space for the lithosphere, ${}_0D_t^{\alpha}$ is the Caputo fractional operator (Caputo, 1967) defined as equation (6) such that α, $(0 < \alpha \leq 1)$ is the order of fractional derivatives and 0, t are lower and upper limits, respectively.

2.3.2 Stress equation of motion:

For the fault F_1, the equation is

$$\frac{\partial}{\partial y_2}(\tau_{12}) + \frac{\partial}{\partial y_3}(\tau_{13}) = 0 \quad (13)$$

and for the fault F_2, these are

$$\sum_{j=1}^{3}\frac{\partial \tau_{ij}}{\partial y_j} = 0, i = 1,2,3 \quad (14)$$

where $-\infty < y_2 < \infty, y_3 \geq 0$ and $t \geq 0$.

2.3.3 Boundary Conditions:

Here, we consider a situation where fault F_1 moves earlier than fault F_2. As a result, the boundary conditions are applied exclusively across fault F_1 and are taken to be the same as (8)-(10).

2.3.4 Initial conditions:

At time $t = 0$, the displacement, stress and strain components are assumed to be $(u_1)_0$, $(\tau_{12})_0$, $(\tau_{13})_0$, $(e_{12})_0$, $(e_{13})_0$, respectively while that for finite fault F_2 be $(u_i)_0$, $(\tau_{ij})_0$ and $(e_{ij})_0$, respectively $(i,j = 1,2,3)$. All of them will satisfy the equations (11)-(14).

3 Solution

In the following sections, we have solved the boundary value problems above, before and after the movement of the faults for both cases.

3.1 Case-I: Both F_1 and F_2 are infinite:

Differentiating (5) partially with respect to y_2 and y_3 respectively for values of $j = 2, 3$, and using the relations (7), we get

$$\nabla^2 \left(\mu + 2\eta\, {}_0D_t^{\alpha}\right) u_1 = 0, \text{ where } \nabla^2 \equiv \frac{\partial^2}{\partial y_2^2} + \frac{\partial^2}{\partial y_3^2}$$

Taking the Laplace transformation and neglecting the 1st and higher order derivatives of u_1, we get

$$\mu \nabla^2 \{\overline{u_1}(s)\} + 2\eta \left[s^{\alpha} \nabla^2 \{\overline{u_1}(s)\} - s^{\alpha-1} \nabla^2 (u_1)_0\right] = 0$$

The inverse Laplace transformation of the above equation gives

$$\nabla^2 U = 0, \text{ where } U = u_1 - E_{\alpha}\left(-\frac{\mu}{2\eta} t^{\alpha}\right)(u_1)_0 \tag{15}$$

Here, $E_{\alpha}\left(-\frac{\mu}{2\eta} t^{\alpha}\right)$ represents Mittag-Leffler function proposed by Mittag-Leffler (1903).

3.1.1 Solution before fault creep:

The solutions for displacement, stresses, and strains before fault creep can be found by solving the above boundary value problem (5) to (10). Taking Laplace transformation with respect to time on the equations (5) (for $j = 2, 3$) (the first and higher-order time derivatives of τ_{12}, τ_{13} and u_1 can be neglected due to their insignificance in the range $0 < \alpha < 1$), stress-equation of motion (7), boundary conditions (8) to (10) and governing equation (15), we get

$$\overline{\tau_{1j}} = \frac{\frac{\eta}{\mu} s^{\alpha-1}}{1 + \frac{\eta}{\mu} s^{\alpha}} (\tau_{1j})_0 + \frac{1}{1 + \frac{\eta}{\mu} s^{\alpha}} \frac{\partial}{\partial y_j} \left\{\left(\mu + 2\eta s^{\alpha}\right) \overline{u}_1 - 2\eta s^{\alpha-1} (u_1)_0\right\};\ j = 2, 3 \tag{16}$$

$$\frac{\partial}{\partial y_2}(\overline{\tau_{12}}) + \frac{\partial}{\partial y_3}(\overline{\tau_{13}}) = 0 \tag{17}$$

$$\begin{cases} \overline{\tau_{12}} \to \tau_{\infty}(0)\left(\frac{1}{s} + \frac{k}{s^2}\right) \text{ as } |y_2| \to \infty,\ y_3 \geq 0,\ t \geq 0,\ k > 0 \\ \overline{\tau_{13}} \to 0 \text{ as } y_3 \to \infty,\ -\infty < y_2 < \infty,\ t \geq 0 \\ \overline{\tau_{13}} = 0 \text{ on } y_3 = 0,\ -\infty < y_2 < \infty,\ t \geq 0 \end{cases} \tag{18}$$

and

$$\nabla^2 \overline{U} = 0, \quad \text{where} \quad \overline{U} = \overline{u_1} - \frac{s^{\alpha-1}}{s^{\alpha} + \frac{\mu}{2\eta}} (u_1)_0 \tag{19}$$

where $\overline{\tau_{12}}$, $\overline{\tau_{13}}$, $\overline{U}$, $\overline{u_1}$ represents the Laplace transforms of τ_{12}, τ_{13}, U, u_1 respectively for time t, and s denotes the corresponding Laplace transform parameter.

Let the trial solution of (19) be

$$\overline{U} = Ay_2 + By_3 \quad \text{i.e.,} \quad \overline{u_1}(y_2, y_3, s) = \frac{s^{\alpha-1}}{(s^\alpha + \frac{\mu}{2\eta})}(u_1)_0 + Ay_2 + By_3 \tag{20}$$

where the unknowns A and B may be constants or functions of s only and are independent of the space coordinates y_2, y_3.
If we substitute the expression of $\overline{u_1}$ from (20) in the equations (16) and use the boundary conditions (18), we will have the unknown A and B as

$$\begin{cases} A = \frac{\tau_\infty(0)}{\mu + 2\eta s^\alpha}\left[\frac{1}{s} + \frac{k}{s^2} + \frac{\eta k}{\mu}s^{\alpha-2}\right] \\ B = 0 \end{cases} \tag{21}$$

Hence, substituting these expressions of A and B in (20), we have

$$\overline{u_1} = \frac{s^{\alpha-1}}{(s^\alpha + \frac{\mu}{2\eta})}(u_1)_0 + \frac{\tau_\infty(0)y_2}{\mu + 2\eta s^\alpha}\left[\frac{1}{s} + \frac{k}{s^2} + \frac{\eta k}{\mu}s^{\alpha-2}\right] \tag{22}$$

Now, substituting the expression of (22) in (16) (for $j = 2, 3$) and taking the inverse Laplace transformation of the resulting relations, including (22), we get the solution before fault creep as

$$\begin{cases} u_1 = (u_1)_0 E_\alpha\left(-\frac{\mu}{2\eta}t^\alpha\right) + \frac{y_2\tau_\infty(0)}{\mu}\left[\left(1 - \frac{\eta k}{\mu}\right)\left(1 - E_\alpha\left(-\frac{\mu}{2\eta}t^\alpha\right)\right) + kt\right] \\ \tau_{12} = (\tau_{12})_0 E_\alpha\left(-\frac{\mu}{\eta}t^\alpha\right) + \tau_\infty(0)\left[1 + kt - E_\alpha\left(-\frac{\mu}{\eta}t^\alpha\right)\right] \\ \tau_{13} = (\tau_{13})_0 E_\alpha\left(-\frac{\mu}{\eta}t^\alpha\right) \\ e_{12} = \frac{\partial u_1}{\partial y_2} = (e_{12})_0 E_\alpha\left(-\frac{\mu}{2\eta}t^\alpha\right) + \frac{\tau_\infty(0)}{\mu}\left[\left(1 - \frac{\eta k}{\mu}\right)\left(1 - E_\alpha\left(-\frac{\mu}{2\eta}t^\alpha\right)\right) + kt\right] \\ e_{13} = \frac{\partial u_1}{\partial y_3} = (e_{13})_0 E_\alpha\left(-\frac{\mu}{2\eta}t^\alpha\right) \end{cases} \tag{23}$$

The shear stress component τ'_{12} acting along fault F_1, responsible for initiating strike-slip motion, is expressed as follows:

$$\tau'_{12} = (\tau'_{12})_0 E_\alpha\left(-\frac{\mu}{\eta}t^\alpha\right) + \tau_\infty(t)\sin\theta_1 - \tau_\infty(0)\sin\theta_1 E_\alpha\left(-\frac{\mu}{\eta}t^\alpha\right) \tag{24}$$

where $(\tau'_{12})_0 = (\tau_{12})_0 \sin\theta_1 - (\tau_{13})_0 \cos\theta_1$ is the value of τ'_{12} at $t = 0$.

We observe that for the fault F_1 if shear stress τ'_{12} near the fault F_1 is less than

$\tau_\infty(t)\sin\theta_1$, then shear stress τ'_{12} accumulate continuously and τ'_{12} approaches to $\tau_\infty(t)\sin\theta_1$ as $t \to \infty$. If the property of the fault is such that as the shear stress τ'_{12} near the fault F_1 exceeds the critical value, say τ_{c_1} $(< \tau_\infty(t)\sin\theta_1)$, then there will be a movement along the fault F_1 after a finite length of time say T_1.

Due to strike-slip movement along the faults, seismic waves occur, which gradually disappear over time and restore the aseismic state of the system. During this seismic event, which lasted for a very short interval of time (lasts only a few tens of seconds, but it can last for minutes in the greatest earthquakes), all the boundary conditions were not valid. So, skipping this seismic period, we re-initiate the analysis from the point when the system returns to its aseismic state and set the new time appropriately.

3.1.2 Solution after fault creep:

The characteristic of both faults is assumed in such a way that they both undergo creeping movement (not sudden movement) when the stress near them becomes sufficiently high to overcome the local cohesive and frictional forces. Let the fault F_1 start to creep at an instant $t = T_1\,(> 0)$, while that time for fault F_2 be $t = T_2\,(\geq T_1 > 0)$. All the equations of (5) - (10) (except (8)) are valid for $t \geq T_2 \geq T_1$. Moreover, the faults F_1 and F_2 will satisfy the additional dislocation conditions:

$$[u_1]_{F_1} = U_1(t_1)f_1(y'_3)H(t_1) \text{ across the fault } F_1 : y'_2 = 0, 0 \leq y'_3 \leq D_1, t_1 = t - T_1 \tag{25}$$

and

$$[u_1]_{F_2} = U_2(t_2)f_2(z'_3)H(t_2) \text{ across the fault } F_2 : z'_2 = 0, 0 \leq z'_3 \leq D_2, t_2 = t - T_2 \tag{26}$$

where $U_1(t_1)$ and $U_2(t_2)$ are the slips of F_1 and F_2, respectively. If V_1,V_2 be the creep velocities of the faults F_1 and F_2, respectively then the slip can be expressed as $U_1(t_1) = V_1 t_1$ and $U_2(t_2) = V_2 t_2$.

$f_1(y'_3)$ and $f_2(z'_3)$ are depth-dependence continuous functions of y'_3 and z'_3 denoting the creep functions of the faults F_1 and F_2 respectively. $H(t_i), i = 1, 2$ are Heaviside functions defined as

$$H(t_i) = \begin{cases} 1 \text{ for } t_i \geq 0 \\ 0 \text{ for } t_i < 0 \end{cases} \qquad \text{for } i = 1, 2 \tag{27}$$

and the relative displacements $[u_1]_{F_1}$ and $[u_2]_{F_2}$ across the faults F_1 and F_2 are respectively defined as

$$[u_1]_{F_1} = \lim_{y'_2 \to 0^+}(u_1) - \lim_{y'_2 \to 0^-}(u_1) \tag{28}$$

and

$$[u_1]_{F_2} = \lim_{z_2' \to 0^+} (u_1) - \lim_{z_2' \to 0^-} (u_1) \tag{29}$$

The solutions after the creep of both faults can be written in the following format.

$$\begin{cases} u_1 = (u_1)_1 + (u_1)_2 + (u_1)_3 \\ \tau_{12} = (\tau_{12})_1 + (\tau_{12})_2 + (\tau_{12})_3 \\ \tau_{13} = (\tau_{13})_1 + (\tau_{13})_2 + (\tau_{13})_3 \\ e_{12} = (e_{12})_1 + (e_{12})_2 + (e_{12})_3 \\ e_{13} = (e_{13})_1 + (e_{13})_2 + (e_{13})_3 \end{cases} \tag{30}$$

where $(u_1)_1, (\tau_{12})_1$, $(\tau_{13})_1$, $(e_{12})_1$ and $(e_{13})_1$ are similar to the components of displacement, stress and strain in the absence of any fault movement as mentioned in (23). These components are due to the effect of the initial field concerning time origin and the tectonic forces due to mantle convection. $(u_1)_2, (\tau_{12})_2$, $(\tau_{13})_2$, $(e_{12})_2$ and $(e_{13})_2$ represent displacement, stress and strain components due to the effect of the fault movement across the fault F_1. They all are zero for $t_1 < 0$ and satisfy all the relations (5) - (10) and (25) for $t_1 \geq 0$, except the boundary condition (8), which is replaced by

$$(\tau_{12})_2 \to 0 \text{ as } |y_2| \to \infty, y_3 \geq 0, t_1 \geq 0 \tag{31}$$

and $(u_1)_3, (\tau_{12})_3$, $(\tau_{13})_3$, $(e_{12})_3$ and $(e_{13})_3$ represent the corresponding components due to the effect of the fault movement across the fault F_2. They are also all zero for $t_2 < 0$ and satisfy all the relations (5), (7) - (10) and (26) for $t_2 \geq 0$, except the boundary condition (8), which is replaced by

$$(\tau_{12})_3 \to 0 \text{ as } |z_2| \to \infty, z_3 \geq 0, t_2 \geq 0 \tag{32}$$

To solve this boundary value problem for $(u_1)_2, (\tau_{12})_2$, $(\tau_{13})_2$, $(e_{12})_2$ and $(e_{13})_2$, we take the Laplace transformation on the relations (5), (7) - (10) (except (8)) with (25) and (31) with respect to $t_1 \geq 0$ and get

$$\overline{(\tau_{1j})}_2 = 2\mu . \frac{p^\alpha + \frac{\mu}{2\eta}}{p^\alpha + \frac{\mu}{\eta}} \frac{\partial \overline{(u_1)}_2}{\partial y_j}; \; j = 2, 3 \tag{33}$$

$$\frac{\partial}{\partial y_2} \overline{(\tau_{12})}_2 + \frac{\partial}{\partial y_3} \overline{(\tau_{13})}_2 = 0 \tag{34}$$

$$\begin{cases} \overline{(\tau_{13})}_2 \to 0 \text{ as } \; y_3 \to \infty, -\infty < y_2 < \infty \\ \overline{(\tau_{13})}_2 = 0 \text{ on } y_3 = 0, -\infty < y_2 < \infty \\ \overline{(\tau_{12})}_2 \to 0 \text{ as } \; |y_2| \to \infty, y_3 \geq 0 \end{cases} \tag{35}$$

where p is the Laplace transform variable with respect to variable t_1.

The above BVP (Boundary Value Problem) is solved with the help of Modified Green's function technique, as proposed by Maruyama (1966), and correspondence principle (Rybicki 1971), which states that if $P(\xi_1, \xi_2, \xi_3)$ be any arbitrary point on the fault F_1 such that $0 < \xi_2 < D_1 \cos\theta_1$, $0 < \xi_3 < D_1 \sin\theta_1$ and $\xi_2 = \xi_3 \cot\theta_1$ and $Q(y_1, y_2, y_3)$ be any arbitrary point on the half-space then dislocation

$$\overline{(u_1)}_2(Q) = \int_{F_1} \overline{(u_1)}_2(P) \{G_{12}(P,Q)d\xi_3 - G_{13}(P,Q)d\xi_2\} \tag{36}$$

where

$$G_{12} = \frac{1}{2\pi}\left[\frac{y_2 - \xi_2}{L^2} + \frac{y_2 - \xi_2}{M^2}\right] \quad \text{and} \quad G_{13} = \frac{1}{2\pi}\left[\frac{y_3 - \xi_3}{L^2} + \frac{y_3 + \xi_3}{M^2}\right] \tag{37}$$

such that

$$L^2 = (y_2 - \xi_2)^2 + (y_3 - \xi_3)^2 \quad \text{and} \quad M^2 = (y_2 - \xi_2)^2 + (y_3 + \xi_3)^2 \tag{38}$$

Let the coordinate system (ξ_1, ξ_2, ξ_3) be transformed to (ξ_1', ξ_2', ξ_3') as

$$\begin{cases} \xi_1 = \xi_1' \\ \xi_2 = \xi_2' \sin\theta_1 + \xi_3' \cos\theta_1 \\ \xi_3 = d_1 - \xi_2' \cos\theta_1 + \xi_3' \sin\theta_1 \end{cases} \tag{39}$$

such that on the fault F_1, $\xi_2' = 0$ and $0 < \xi_3' \leq D_1$.

Putting all the required expressions in (36), we get

$$\overline{(u_1)}_2 = \frac{V_1}{2\pi p^2}\Psi_1(y_2, y_3) \tag{40}$$

where

$$\Psi_1(y_2, y_3) = \int_0^{D_1} f_1(\xi_3') \left[\frac{y_2 \sin\theta_1 - (y_3 - d_1)\cos\theta_1}{{\xi_3'}^2 - 2\xi_3'\{y_2\cos\theta_1 + (y_3 - d_1)\sin\theta_1\} + y_2^2 + (y_3 - d_1)^2}\right.$$
$$\left. + \frac{y_2 \sin\theta_1 + (y_3 + d_1)\cos\theta_1}{{\xi_3'}^2 - 2\xi_3'\{y_2\cos\theta_1 - (y_3 + d_1)\sin\theta_1\} + y_2^2 + (y_3 + d_1)^2}\right] d\xi_3' \tag{41}$$

Here is a refined, plagiarism-free version of your sentence:

Furthermore, by substituting the expression for $\overline{(u_1)}_2$ from equation (40) into equation (33), and subsequently applying the inverse Laplace transform, including

(40), we obtain the analytical expressions for the displacement, stress, and strain components resulting from the slip along fault F_1 as

$$\begin{cases} (u_1)_2 = \frac{V_1 t_1}{2\pi} H(t_1)\Psi_1(y_2, y_3) \\ (\tau_{12})_2 = \frac{\mu V_1}{2\pi} H(t_1)\Psi_2(y_2, y_3)\left\{t_1 + \frac{\eta}{\mu}\left(1 - E_\alpha\left(-\frac{\mu}{\eta}t_1^\alpha\right)\right)\right\} \\ (\tau_{13})_2 = \frac{\mu V_1}{2\pi} H(t_1)\Psi_3(y_2, y_3)\left\{t_1 + \frac{\eta}{\mu}\left(1 - E_\alpha\left(-\frac{\mu}{\eta}t_1^\alpha\right)\right)\right\} \\ (e_{12})_2 = \frac{\partial (u_1)_2}{\partial y_2} = \frac{V_1 t_1}{2\pi} H(t_1)\Psi_2(y_2, y_3) \\ (e_{12})_2 = \frac{\partial (u_1)_2}{\partial y_3} = \frac{V_1 t_1}{2\pi} H(t_1)\Psi_3(y_2, y_3) \end{cases} \tag{42}$$

where Ψ_1 is as given in equation (41), $\Psi_2 = \frac{\partial \Psi_1}{\partial y_2}$ and $\Psi_3 = \frac{\partial \Psi_1}{\partial y_3}$.

The movement along the strike of the fault F_2 is induced by

$$\begin{aligned} \tau_{12}'' = (\tau_{12}'')_0 E_\alpha\left(-\frac{\mu}{\eta}t^\alpha\right) + \tau_\infty(0)\sin\theta_2\left\{1 + kt - E_\alpha\left(-\frac{\mu}{\eta}t^\alpha\right)\right\} \\ + \frac{\mu V_1}{2\pi} H(t_1)\left\{t_1 + \frac{\eta}{\mu}\left(1 - E_\alpha\left(-\frac{\mu}{\eta}t_1^\alpha\right)\right)\right\}(\Psi_2 \sin\theta_2 - \Psi_3 \cos\theta_2) \end{aligned} \tag{43}$$

where $(\tau_{12}'')_0 = (\tau_{12})_0 \sin\theta_2 - (\tau_{13})_0 \cos\theta_2$.

Then by following exactly the similar process, for the fault F_2, the displacement component $(u_1)_3$, stresses components $(\tau_{12})_3$, $(\tau_{13})_3$ and strain components $(e_{12})_3$, $(e_{13})_3$ due to the effect of the movement of the infinite fault F_2 can be computed as

$$\begin{cases} (u_1)_3 = \frac{V_2 t_2}{2\pi} H(t_2)\Phi_1(y_2, y_3) \\ (\tau_{12})_3 = \frac{\mu V_2}{2\pi} H(t_2)\Phi_2(y_2, y_3)\left\{t_2 + \frac{\eta}{\mu}\left(1 - E_\alpha\left(-\frac{\mu}{\eta}t_2^\alpha\right)\right)\right\} \\ (\tau_{13})_3 = \frac{\mu V_2}{2\pi} H(t_2)\Phi_3(y_2, y_3)\left\{t_2 + \frac{\eta}{\mu}\left(1 - E_\alpha\left(-\frac{\mu}{\eta}t_2^\alpha\right)\right)\right\} \\ (e_{12})_3 = \frac{V_2 t_2}{2\pi} H(t_2)\Phi_2(y_2, y_3) \\ (e_{12})_3 = \frac{V_2 t_3}{2\pi} H(t_2)\Phi_3(y_2, y_3) \end{cases} \tag{44}$$

where (z_1, z_2, z_3) be a field point such that $z_2 = y_2 - D, z_3 = y_3$ on half-space and the fault point (η_1, η_2, η_3) is transformed to $(\eta_1', \eta_2', \eta_3')$ such that

$$\begin{cases} \eta_1 = \eta_1' \\ \eta_2 = \eta_2' \sin\theta_2 + \eta_3' \cos\theta_2 \\ \eta_3 = d_2 - \eta_2' \cos\theta_2 + \eta_3' \sin\theta_2 \end{cases} \tag{45}$$

Also,

$$\Phi_1(y_2, y_3) = \int_0^{D_2} f_2(\eta_3')$$

$$\left[\frac{(y_2-D)\sin\theta_2-(y_3-d_2)\cos\theta_2}{{\eta_3'}^2-2\eta_3'\{(y_2-D)\cos\theta_2+(y_3-d_2)\sin\theta_2\}+(y_2-D)^2+(y_3-d_2)^2}\right.$$
$$\left.+\frac{(y_2-D)\sin\theta_2+(y_3-d_2)\cos\theta_2}{{\eta_3'}^2-2\eta_3'\{(y_2-D)\cos\theta_2-(y_3-d_2)\sin\theta_2\}+(y_2-D)^2+(y_3-d_2)^2}\right]d\eta_3' \quad (46)$$

and $\Phi_2=\frac{\partial\Phi_1}{\partial y_2}$, $\Phi_3=\frac{\partial\Phi_1}{\partial y_3}$.

Now, subsisting the values of (23), (42) and (44) in (30), we will have the final solution for displacement, stress, and strains (when both the faults are infinite buried) as below:

$$\begin{cases}
u_1=(u_1)_0E_\alpha\left(-\frac{\mu}{2\eta}t^\alpha\right)+\frac{y_2\tau_\infty(0)}{\mu}\left[\left(1-\frac{\eta k}{\mu}\right)+kt+\left(\frac{\eta k}{\mu}-1\right)E_\alpha\left(-\frac{\mu}{2\eta}t^\alpha\right)\right]\\
\quad+\frac{V_1t_1}{2\pi}H(t_1)\Psi_1(y_2,y_3)+\frac{V_2t_2}{2\pi}H(t_2)\Phi_1(y_2,y_3)\\
\tau_{12}=(\tau_{12})_0E_\alpha\left(-\frac{\mu}{\eta}t^\alpha\right)+\tau_\infty(0)\left[1+kt-E_\alpha\left(-\frac{\mu}{\eta}t^\alpha\right)\right]\\
\quad+\frac{\mu V_1}{2\pi}H(t_1)\Psi_2(y_2,y_3)\left\{t_1+\frac{\eta}{\mu}\left(1-E_\alpha\left(-\frac{\mu}{\eta}t_1^\alpha\right)\right)\right\}\\
\quad+\frac{\mu V_2}{2\pi}H(t_2)\Phi_2(y_2,y_3)\left\{t_2+\frac{\eta}{\mu}\left(1-E_\alpha\left(-\frac{\mu}{\eta}t_2^\alpha\right)\right)\right\}\\
\tau_{13}=(\tau_{13})_0E_\alpha\left(-\frac{\mu}{\eta}t^\alpha\right)+\frac{\mu V_1}{2\pi}H(t_1)\Psi_3(y_2,y_3)\left\{t_1+\frac{\eta}{\mu}\left(1-E_\alpha\left(-\frac{\mu}{\eta}t_1^\alpha\right)\right)\right\}\\
\quad+\frac{\mu V_2}{2\pi}H(t_2)\Phi_3(y_2,y_3)\left\{t_2+\frac{\eta}{\mu}\left(1-E_\alpha\left(-\frac{\mu}{\eta}t_2^\alpha\right)\right)\right\}\\
e_{12}=(e_{12})_0E_\alpha\left(-\frac{\mu}{2\eta}t^\alpha\right)+\frac{\tau_\infty(0)}{\mu}\left[\left(1-\frac{\eta k}{\mu}\right)+kt+\left(\frac{\eta k}{\mu}-1\right)E_\alpha\left(-\frac{\mu}{2\eta}t^\alpha\right)\right]\\
\quad+\frac{V_1t_1}{2\pi}H(t_1)\Psi_2(y_2,y_3)+\frac{V_2t_2}{2\pi}H(t_2)\Phi_2(y_2,y_3)\\
e_{13}=(e_{13})_0E_\alpha\left(-\frac{\mu}{2\eta}t^\alpha\right)+\frac{V_1t_1}{2\pi}H(t_1)\Psi_3(y_2,y_3)+\frac{V_2t_2}{2\pi}H(t_2)\Phi_3(y_2,y_3)
\end{cases} \quad (47)$$

Total driving force across the fault F_1 is derived by the equation $(T_{12}')_I=\tau_{12}\sin\theta_1-\tau_{13}\cos\theta_1$ and is given by

$$\begin{aligned}(T_{12}')_I=&(\tau_{12}')_0\,E_\alpha\left(-\frac{\mu}{2\eta}t^\alpha\right)\sin\theta_1+\tau_\infty(0)\left[1+kt-E_\alpha\left(-\frac{\mu}{\eta}t^\alpha\right)\right]\sin\theta_1\\
&+\frac{\mu V_1}{2\pi}H(t_1)\left\{t_1+\frac{\eta}{\mu}\left(1-E_\alpha\left(-\frac{\mu}{\eta}t_1^\alpha\right)\right)\right\}(\Psi_2\sin\theta_1-\Psi_3\cos\theta_1)\\
&+\frac{\mu V_2}{2\pi}H(t_2)\left\{t_2+\frac{\eta}{\mu}\left(1-E_\alpha\left(-\frac{\mu}{\eta}t_2^\alpha\right)\right)\right\}(\Phi_2\sin\theta_1-\Phi_3\cos\theta_1)\end{aligned} \quad (48)$$

and that along the fault F_2 is given by

$$\begin{aligned}(T_{12}'')_I=&(\tau_{12}'')_0\,E_\alpha\left(-\frac{\mu}{2\eta}t^\alpha\right)\sin\theta_2+\tau_\infty(0)\left[1+kt-E_\alpha\left(-\frac{\mu}{\eta}t^\alpha\right)\right]\sin\theta_2\\
&+\frac{\mu V_1}{2\pi}H(t_1)\left\{t_1+\frac{\eta}{\mu}\left(1-E_\alpha\left(-\frac{\mu}{\eta}t_1^\alpha\right)\right)\right\}(\Psi_2\sin\theta_2-\Psi_3\cos\theta_2)\\
&+\frac{\mu V_2}{2\pi}H(t_2)\left\{t_2+\frac{\eta}{\mu}\left(1-E_\alpha\left(-\frac{\mu}{\eta}t_2^\alpha\right)\right)\right\}(\Phi_2\sin\theta_2-\Phi_3\cos\theta_2)\end{aligned} \quad (49)$$

where $(\tau'_{12})_0 = (\tau_{12})_0 \sin\theta_1 - (\tau_{13})_0 \cos\theta_1$ and $(\tau''_{12})_0 = (\tau_{12})_0 \sin\theta_2 - (\tau_{13})_0 \cos\theta_2$.

3.2 Case-II: F_1 is infinite buried and F_2 is finite surface breaking

3.2.1 Solution before fault creep:

Solution when there is no fault movement (for $t < T_1$, where T_1 is the time when the fault F_1 starts to creep) will be the same as case-I, which is mentioned in equation (23).
Let the fault F_2 move after time $t = T_2\,(> 0)$ such that $T_1 < T_2$.

3.2.2 Solution after fault creep:

The displacement, stress, and strain fields generated after the initiation of slip on faults F_1 and F_2 will be of the form mentioned in (30), where $(u_1)_1, (\tau_{12})_1, (\tau_{13})_1, (e_{12})_1$, $(e_{13})_1$ are same as (23), which represent the effect of the initial field concerning time origin and of the tectonic forces due to mantle convection. $(u_1)_2, (\tau_{12})_2, (\tau_{13})_2, (e_{12})_2$, $(e_{13})_2$ are the same as (42) and represent the effect of the slip of the fault F_1 at time $t = T_1$. Let $(u_1)_3, (\tau_{12})_3, (\tau_{13})_3, (e_{12})_3$, $(e_{13})_3$ represents the effect of the slip of the fault F_2 at time $t = T_2$. Afterwards when the fault F_2 moves, constitutive equations (12) stress-equation of motions (14) remains valid and dislocation condition is given by

$$[u_1]_{F_2} = U_2(t_2) f_2(z'_1, z'_3) H(t_2), \text{ across the fault } F_2 : -L \le z'_1 \le L, z'_2 = 0, \\ 0 \le z'_3 \le D_2, t_2 = t - T_2 \quad (50)$$

Here, $f_2(z'_1, z'_3)$ is the creep function across the fault and $[u_1]_{F_2}$ is the discontinuity in displacement along F_2 defined by

$$[u_1]_{F_2} = \lim_{z'_2 \to 0^+} (u_1) - \lim_{z'_2 \to 0^-} (u_1) \quad (51)$$

The additional boundary condition is

$$(\tau_{12})_3 \to 0 \text{ as } |z_2| \to \infty,\ z_3 \ge 0,\ t_2 \ge 0 \quad (52)$$

Let V_2 be the prescribed creep velocity associated to the fault F_2, then $U_2(t_2) = V_2 t_2$. The fault creep commences across the fault F_2 after time $t = T_2$. So, $[u_1]_{F_2} = 0$ for $t_2 = t - T_2 \le 0$. Hence for $t_2 > 0$, we can write the equation (50) as

$$[u_1]_{F_2} = V_2 t_2 f_2(z'_1, z'_3) H(t_2); -L \le z'_1 \le L, z'_2 = 0, 0 \le z'_3 \le D_2, t_2 = t - T_2 \quad (53)$$

To get the solutions, Laplace transformation of all the equations (12), (14) (for $i, j = 1, 2, 3$) and (52), (53), respectively for $t_2 \ge 0$, which gives

$$\overline{(\tau_{ij})}_3 = 2\mu . \frac{p^\alpha + \frac{\mu}{2\eta}}{p^\alpha + \frac{\mu}{\eta}} \frac{\partial \overline{(u_i)}_3}{\partial y_j}; i, j = 1, 2, 3 \quad (54)$$

$$\sum_{j=1}^{3} \frac{\partial \overline{(\tau_{ij})}_3}{\partial y_j} = 0; i = 1, 2, 3 \tag{55}$$

$$\overline{(\tau_{12})}_3 \to 0 \text{ as } |y_2| \to \infty,\ y_3 \geq 0,\ t \geq 0 \tag{56}$$

$$\overline{[u_1]}_{F_2} = \frac{V_2}{p^2} f_2(z_1', z_3') \tag{57}$$

Let $Q(z_1, z_2, z_3)$ be an arbitrary point in the half-space and $P(\eta_1, \eta_2, \eta_3)$ be any point on the fault F_2, then using Green's function technique proposed by Maruyama (1966) together with the correspondence principle proposed by Rybicki (1971), we get the dislocation function as

$$\overline{(u_1)}_3 = \int\int_{F_2} \overline{[u_1]}_{F_2} G(P, Q) d\eta_1 \eta_3 \tag{58}$$

such that $G(P, Q)$ represents Green's function and is defined as $G(P, Q) = \frac{\partial}{\partial \eta_2} G_1(P, Q)$ such that $G_1(P, Q) = \left[\frac{1}{[(z_1-\eta_1)^2+(z_2-\eta_2)^2+(z_3-\eta_3)^2]^{\frac{1}{2}}} - \frac{1}{[(z_1+\eta_1)^2+(z_2-\eta_2)^2+(z_3-\eta_3)^2]^{\frac{1}{2}}} \right]$. Transformation of the coordinate system (η_1, η_2, η_3) to $(\eta_1', \eta_2', \eta_3')$ is taken as

$$\begin{cases} \eta_1 = \eta_1' \\ \eta_2 = \eta_2' \sin\theta_2 + \eta_3' \cos\theta_2 \\ \eta_3 = -\eta_2' \cos\theta_2 + \eta_3' \sin\theta_2 \end{cases} \tag{59}$$

such that on the fault F_2, $\eta_2' = 0$
Substituting all the required expressions in (58), we get

$$\overline{(u_1)}_3 = \frac{V_2}{p^2} \Phi_1(y_1, y_2, y_3) \tag{60}$$

where

$$\Phi_1 = \int_0^{D_2} \int_{-L}^{L} f_2(\eta_1', \eta_3') \left[\frac{y_2 - D - \eta_3' \cos\theta_2}{M^{\frac{3}{2}}} - \frac{y_2 - D - \eta_3' \cos\theta_2}{N^{\frac{3}{2}}} \right] \sin\theta_2 d\eta_1' d\eta_3' \tag{61}$$

and $M = (y_1 - \eta_1')^2 + (y_2 - D - \eta_3' \cos\theta_2)^2 + (y_3 - \eta_3' \sin\theta_2)^2$,
$N = (y_1 + \eta_1')^2 + (y_2 - D - \eta_3' \cos\theta_2)^2 + (y_3 - \eta_3' \sin\theta_2)^2$.

By substituting the expression of (60) in (54) and then applying the inverse Laplace

transformation, the displacement, stress, and finally strain fields induced by the slip of the fault F_2 is expressed as

$$\begin{cases} (u_1)_3 = V_2 t_2 H(t_2)\Phi_1(y_1,y_2,y_3) \\ (u_2)_3 = (u_3)_3 = 0 \\ (\tau_{11})_3 = \mu V_2 H(t_2)\Phi_2(y_1,y_2,y_3)\left\{t_2 + \frac{\eta}{\mu}\left(1 - E_\alpha\left(-\frac{\mu}{\eta}t_2^\alpha\right)\right)\right\} \\ (\tau_{12})_3 = \frac{\mu V_2}{2} H(t_2)\Phi_3(y_1,y_2,y_3)\left\{t_2 + \frac{\eta}{\mu}\left(1 - E_\alpha\left(-\frac{\mu}{\eta}t_2^\alpha\right)\right)\right\} \\ (\tau_{13})_3 = \frac{\mu V_2}{2} H(t_2)\Phi_4(y_1,y_2,y_3)\left\{t_2 + \frac{\eta}{\mu}\left(1 - E_\alpha\left(-\frac{\mu}{\eta}t_2^\alpha\right)\right)\right\} \\ (\tau_{22})_3 = (\tau_{23})_3 = (\tau_{33})_3 = 0 \end{cases} \tag{62}$$

where Φ_1 s as given in (61) and $\Phi_2 = \frac{\partial \Phi_1}{\partial y_1}, \Phi_3 = \frac{\partial \Phi_1}{\partial y_2}, \Phi_4 = \frac{\partial \Phi_1}{\partial y_3}$.

Hence, the complete solution for the displacement, stress and strain components for case-II, is as given below:

$$\begin{cases} u_1 = (u_1)_0 E_\alpha\left(-\frac{\mu}{2\eta}t^\alpha\right) + \frac{y_2\tau_\infty(0)}{\mu}\left[\left(1 - \frac{\eta k}{\mu}\right) + kt + \left(\frac{\eta k}{\mu} - 1\right)E_\alpha\left(-\frac{\mu}{2\eta}t^\alpha\right)\right] \\ \quad + \frac{V_1 t_1}{2\pi} H(t_1)\Psi_1(y_2,y_3) + V_2 t_2 H(t_2)\Phi_1(y_1,y_2,y_3) \\ u_2 = u_3 = 0 \\ \tau_{11} = \mu V_2 H(t_2)\Phi_2(y_1,y_2,y_3)\left\{t_2 + \frac{\eta}{\mu}\left(1 - E_\alpha\left(-\frac{\mu}{\eta}t_2^\alpha\right)\right)\right\} \\ \tau_{12} = (\tau_{12})_0 E_\alpha\left(-\frac{\mu}{\eta}t^\alpha\right) + \tau_\infty(0)\left[1 + kt - E_\alpha\left(-\frac{\mu}{\eta}t^\alpha\right)\right] \\ \quad + \frac{\mu V_1}{2\pi} H(t_1)\Psi_2(y_2,y_3)\left\{t_1 + \frac{\eta}{\mu}\left(1 - E_\alpha\left(-\frac{\mu}{\eta}t_1^\alpha\right)\right)\right\} \\ \quad + \frac{\mu V_2}{2} H(t_2)\Phi_3(y_1,y_2,y_3)\left\{t_2 + \frac{\eta}{\mu}\left(1 - E_\alpha\left(-\frac{\mu}{\eta}t_2^\alpha\right)\right)\right\} \\ \tau_{13} = (\tau_{13})_0 E_\alpha\left(-\frac{\mu}{\eta}t^\alpha\right) + \frac{\mu V_1}{2\pi} H(t_1)\Psi_3(y_2,y_3)\left\{t_1 + \frac{\eta}{\mu}\left(1 - E_\alpha\left(-\frac{\mu}{\eta}t_1^\alpha\right)\right)\right\} \\ \quad + \frac{\mu V_2}{2} H(t_2)\Phi_4(y_1,y_2,y_3)\left\{t_2 + \frac{\eta}{\mu}\left(1 - E_\alpha\left(-\frac{\mu}{\eta}t_2^\alpha\right)\right)\right\} \\ \tau_{22} = \tau_{23} = \tau_{33} = 0 \\ e_{11} = (e_{11})_0 E_\alpha\left(-\frac{\mu}{2\eta}t^\alpha\right) + V_2 t_2 H(t_2)\Phi_2(y_1,y_2,y_3) \\ e_{12} = (e_{12})_0 E_\alpha\left(-\frac{\mu}{2\eta}t^\alpha\right) + \frac{\tau_\infty(0)}{\mu}\left[\left(1 - \frac{\eta k}{\mu}\right) + kt + \left(\frac{\eta k}{\mu} - 1\right)E_\alpha\left(-\frac{\mu}{2\eta}t^\alpha\right)\right] \\ \quad + \frac{V_1 t_1}{2\pi} H(t_1)\Psi_2(y_2,y_3) + \frac{V_2 t_2}{2} H(t_2)\Phi_3(y_1,y_2,y_3) \\ e_{13} = (e_{13})_0 E_\alpha\left(-\frac{\mu}{2\eta}t^\alpha\right) + \frac{V_1 t_1}{2\pi} H(t_1)\Psi_3(y_2,y_3) + \frac{V_2 t_2}{2} H(t_2)\Phi_4(y_1,y_2,y_3) \\ e_{22} = e_{23} = e_{33} = 0 \end{cases} \tag{63}$$

Similar to case-I, in this case, the driving force act on the fault F_1 is expressed as

$$\begin{aligned} (T'_{12})_{II} = (\tau'_{12})_0 E_\alpha\left(-\frac{\mu}{2\eta}t^\alpha\right)\sin\theta_1 + \tau_\infty(0)\left[1 + kt - E_\alpha\left(-\frac{\mu}{\eta}t^\alpha\right)\right]\sin\theta_1 \\ + \frac{\mu V_1}{2\pi} H(t_1)\left\{t_1 + \frac{\eta}{\mu}\left(1 - E_\alpha\left(-\frac{\mu}{\eta}t_1^\alpha\right)\right)\right\}(\Psi_2\sin\theta_1 - \Psi_3\cos\theta_1) \end{aligned}$$

$$+\frac{\mu V_2}{2}H(t_2)\left\{t_2+\frac{\eta}{\mu}\left(1-E_\alpha\left(-\frac{\mu}{\eta}t_2^\alpha\right)\right)\right\}(\Phi_3\sin\theta_1-\Phi_4\cos\theta_1) \quad (64)$$

and is across the fault F_2 is given by

$$\begin{aligned}(T''_{12})_{II} &= (\tau''_{12})_0\,E_\alpha\left(-\frac{\mu}{2\eta}t^\alpha\right)\sin\theta_2+\tau_\infty(0)\left[1+kt-E_\alpha\left(-\frac{\mu}{\eta}t^\alpha\right)\right]\sin\theta_2\\ &+\frac{\mu V_1}{2\pi}H(t_1)\left\{t_1+\frac{\eta}{\mu}\left(1-E_\alpha\left(-\frac{\mu}{\eta}t_1^\alpha\right)\right)\right\}(\Psi_2\sin\theta_2-\Psi_3\cos\theta_2)\\ &+\frac{\mu V_2}{2}H(t_2)\left\{t_2+\frac{\eta}{\mu}\left(1-E_\alpha\left(-\frac{\mu}{\eta}t_2^\alpha\right)\right)\right\}(\Phi_3\sin\theta_2-\Phi_3\cos\theta_4) \quad (65)\end{aligned}$$

where $(\tau'_{12})_0=(\tau_{12})_0\sin\theta_1-(\tau_{13})_0\cos\theta_1$ and $(\tau''_{12})_0=(\tau_{12})_0\sin\theta_2-(\tau_{13})_0\cos\theta_2$.

4 Numerical Computation

The primary focus of developing this mathematical model of interacting faults is to examine the effect of the creeping fault motion on the components of displacement, stress, and strain fields after the restoration of both fault movements, considering different fault inclinations, creep velocities, and order of the fractional derivative. The values of model parameters were selected based on previously published research and field data from real-world geological scenarios, as listed below.

The rigidity modulus μ represents the elastic resistance of crustal rocks to deformation. Rocks commonly found in the Earth's crust, such as granite and basalt, typically exhibit rigidity values between 10^{10} and $10^{11}\,\mathrm{N/m^2}$ (Turcotte and Schubert, 2002). Following Kundu and Sarkar (Mondal) (2020), this study uses an effective rigidity of $\mu=3.5\times10^{10}\,\mathrm{N/m^2}$.
The estimated range of viscosity in lower crust is $10^{16}-10^{21}$ Pa·s (Bischoff and Flesch, 2018) and that is for upper crust is $10^{16}-10^{21}$ Pa·s (Ge et al., 2022). Guided by these findings, we adopt an effective viscosity of $\eta=5\times10^{19}$ Pa·s in our analysis. According to Petersen (1996), the horizontal separation between the upper edges of two faults generally ranging from approximately 8 to 20 km. in regions where they are nearest. In this study, we consider the horizontal distance $D=8$ km.
For case-I, the depths of the faults F_1 and F_2 are assumed to be $d_1=1$ km and $d_2=2$ km, respectively. and for case-II, the depth of fault F_1 is considered to be $d_1=1$ km. These values ensure that faults are located within the continental crust.
For the Case-II, the lengths of the finite faults F_2 is assumed to be $2L_1=20$ km. This value is consistent with observed fault lengths, which commonly range between 15 and 60 km. For instance, the width of the Atacama fault is approximately 50 km. The widths of both the for both cases are taken as $D_1=D_2=10$ km. This choice falls within the typical range of fault widths observed in nature, for example, the San Andreas Fault has estimated widths ranging from 5 to 15 km.
The value of the constant $k=10^{-9}$ is adopted in accordance with the recommendation of Mahato et al. (2022). This choice aligns with the assumption that the tectonic stress $\tau_\infty(t)$ increases gradually in a linear manner over time, as reflected in the

selected boundary conditions.
Since the parameter α lies within the interval $(0, 1]$, we examine the values $\alpha = 0.1,\ 0.4,\ 0.7\,1$ for our analysis.
The fault inclinations θ_1 and θ_2 are restricted to the range $0 < \theta_1, \theta_2 \leq \frac{\pi}{2}$. For graphical purposes, we focus on four specific inclination angles: $\theta_1, \theta_2 = \frac{\pi}{6}, \frac{\pi}{4}, \frac{\pi}{3}, \frac{\pi}{2}$.
Titus et al. (2006) reported that fault creep velocities typically range from 21 to 41 mm/year. In accordance with this, and considering that both faults in our model are characterized as creeping, we assign creep velocities V_1 and V_2 values of 0.02, 0.03, and 0.04 meters/year. These values fall within or closely approximate the observed range.
Following Kundu and Sarkar (2020), the other parametric values are taken as below
Initial stresses $((\tau_{12})_0, (\tau_{13})_0) = 20 \times 10^5$ N/m^2.
Initial stress at infinity $(\tau_\infty(0)) = 20 \times 10^5$ N/m^2.
Commencement time of movement of fault F_1, $T_1 = 50$ years.
Commencement time of movement of fault F_2, $T_2 = 100$ years.
The creep functions when both the faults are infinite:
For the fault F_1, $f_1(y_3') = R_1 \left(1 - \frac{3{y_3'}^2}{D_1^2} + \frac{2{y_3'}^3}{D_1^3}\right)$.
For the fault F_2, $f_2(z_3') = R_2 \left(1 - \frac{3{z_3'}^2}{D_2^2} + \frac{2{z_3'}^3}{D_2^3}\right)$.
The creep functions when the first fault is infinite and the second is finite:
for the fault F_1, $f_1(y_3') = R_1 \left(1 - \frac{3{y_3'}^2}{D_1^2} + \frac{2{y_3'}^3}{D_1^3}\right)$.
For the fault F_2, $f_2(z_1', z_3') = R_2 \left(1 - \frac{1}{L^2{z_1'}^2}\right)\left(1 - \frac{3{z_3'}^2}{D_2^2} + \frac{2{z_3'}^3}{D_2^3}\right)$.
where R_1 and R_2 are constants and carry the values 1 meter. For these creep functions, displacement stresses and strains remain finite.

Change of surface displacement:
Changes of this surface displacement against y_2 for different inclinations due to the slip of the fault F_1 alone are shown in figure 2 taking fixed $V_1 = 0.01$ m/year. It has been observed from the figure that the pattern of changes of displacement is almost similar for each angle of inclination, but the magnitude of surface displacement is different for different inclinations. The peak of the displacement is attained closer to the fault ($y_2 = 0$), and it steadily diminishes on both sides at different rates for different inclinations. As θ_1 increases, the highest magnitude of the displacement decreases. For $y_2 > 0$, this highest magnitude for angles $\pi/6, \pi/4, \pi/3$ and $\pi/2$ are approx. 4.92×10^{-3} m/year, 4.22×10^{-3} m/year, 3.55×10^{-3} m/year and 2.36×10^{-3} m/year respectively. This is consistent with real-world data, such as the displacement rate observed for strike-slip faults is approximately 2-6 mm/year (according to USGS report). As $|y_2| \to \infty$ displacement tends to zero for each inclination. This aligns well with empirical observations and theoretical expectations reported in previous studies (Segall, 2010).

Changes in surface displacement against y_2 due to the movement across both the faults have been shown in figure 3a and 3b for different θ_1 taking fixed $\theta_2 = \pi/3$ when (a) both faults are infinite (case-I), and (b) first fault is infinite second fault finite (case-II). The creep velocities $V_1 = 0.01$ m/year and $V_2 = 0.02$ m/year, respectively.

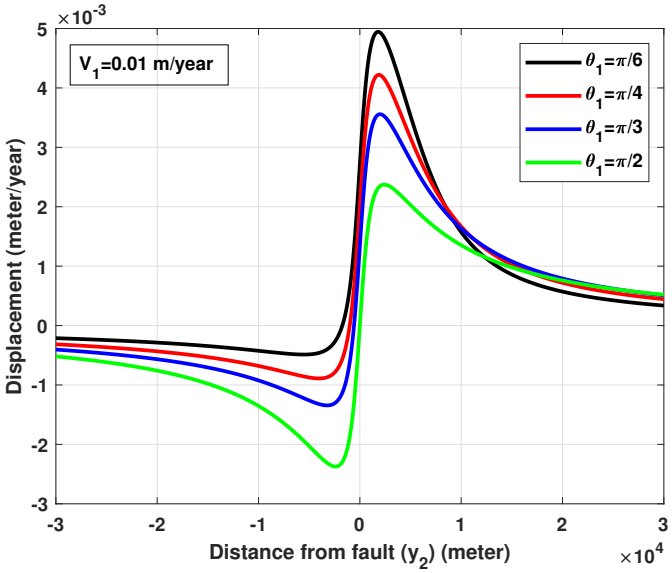


Fig. 2: Variations of surface displacement against y_2 due to the creep on the fault F_1 (with no slip on F_2) for various angle of inclinations of F_1.

Let's compare these figures with figure 2. We can observe that for $y_2 > 0$, for both cases (when both faults are infinite and when one fault is infinite and the other finite), there is an increase in displacement near F_1, which gradually diminishes up to a distance of 8 km from F_1 where the second fault F_2 lies. A sharp increment of displacement is observed again, but it is of different magnitudes for different θ_1. When both the faults are infinite, this maximum magnitude of displacement near F_2 is 1.08×10^{-2} m/year (for $\theta_1 = \pi/4$, figure 3a), while in the other case maximum magnitude near finite fault F_2 is 3.33×10^{-3} m/year (for $\theta = \pi/6$, figure 3b). It is clearly observed that the effect of the movement of both the faults on displacement is more notable in figure 3a near the second fault rather than that in figure 3b. As y_2 increases further, the displacement gradually decreases and ultimately tends to zero as $|y_2| \to \infty$ for both cases. This phenomenon is commensurate with the physical situation. In comparison to the integer-order model introduced by Kundu and Sarkar (Mondal) (2020), their predictions of rate of change of displacement, which is in the range of 10^{-5}, show a notable discrepancy from actual observational data (USGS report), which is of the order of 10^{-3}. This difference in our outcomes may be due to the distinct viscoelastic model and variations in fault geometry employed in our analysis. Also, when compared with one of our previously developed fractional models (Mahato & Sarkar Mondal, 2025), the current model also predicts displacement variations of the order of 10^{-3}. However, a noticeable difference lies in the peak displacement magnitudes produced by the two models. This difference is mainly due to the variation in fault geometry used in the current study.

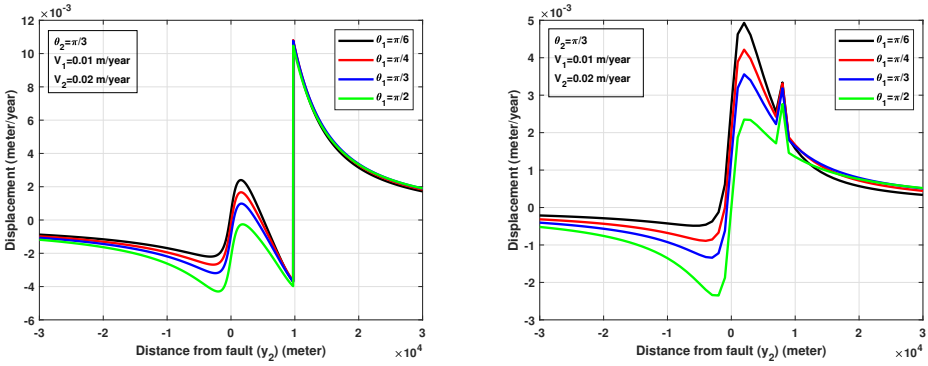


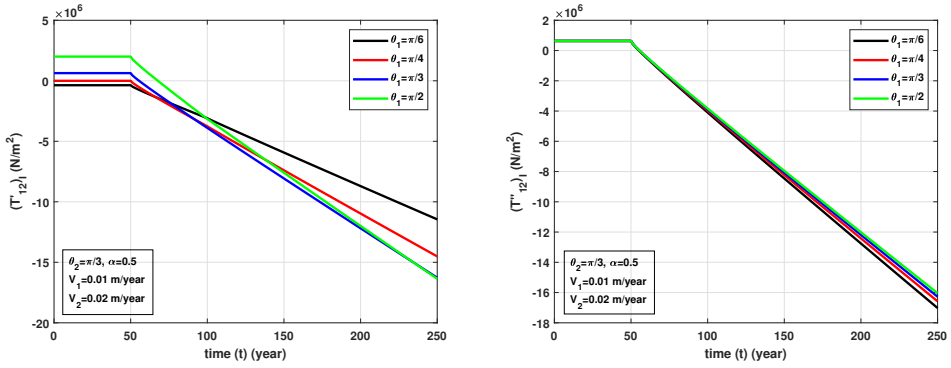
Fig. 3: Change of surface displacement against y_2 for different θ_1 due to creeps across both the faults when (a) both faults are infinite, (b) F_1 is infinite, F_2 is finite.

Variation in the driving force on the free surface resulting from the creeping motion along the fault when both faults are infinite (case-I):

The expression for the total driving force along the fault F_1, when both faults are infinite, is given in (48) and (49). Figures 4a and 4b show the changes in total driving force along the fault F_1 and F_2, respectively, against time for different angles of inclination of the first fault F_1. Here, the fixed inclination of the fault F_2 is $\theta_2 = \pi/3$, $V_1 = 0.01$ m/year, $V_2 = 0.02$ m/year and order of the fraction derivative $\alpha = 0.5$. We observe a few characteristics from the figure 4a. There is a prominent impact of θ_1 on the change in the accumulation/release of the total driving force across F_1. The rate of accumulation is highest for $\theta_1 = \pi/2$ and is lowest for $\theta_1 = \pi/6$, while the rate of release of total driving force across F_1 is different for different θ_1. We also observed that the impact of θ_1 on $(T''_{12})_I$ is not so prominent. A release of driving force has been seen across both faults for different θ_1 with different magnitudes.

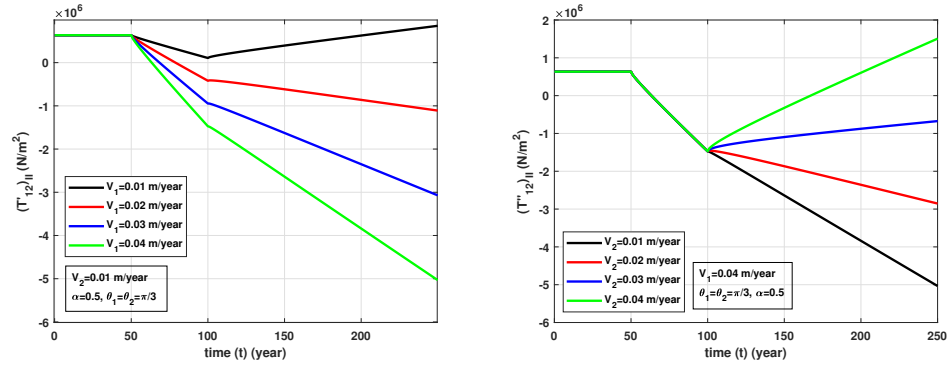
Variation in the driving stress on the free surface caused by the creeping motion along the fault when the first fault is infinite and the second is finite (case-II):

The expression of the total driving force for case-II across faults F_1 and F_2 is given as (64) and (65). Figure 5a shows the change in the total driving force against time across F_1 for different V_1. Here, the effect of different V_1 on driving force is observed after the movement of the fault, i.e., after 50 years. For each creep velocity V_1 except $V_1 = 0.01$ m/year, the driving force releases after a specific time at a different rate. Also, after 100 years (i.e., after the movement of the second fault), this release rate becomes lesser. Figure 5b shows the change of total driving force against time across F_2 for different V_2. A different release rate for different V_2 is observed after 100 years. The magnitude of the release of the driving force in figure 5b is less than that in



(a) (b)

Fig. 4: Variations of total driving force against time for different θ_1 (Case-I) across the fault (a) F_1 (b) F_2.



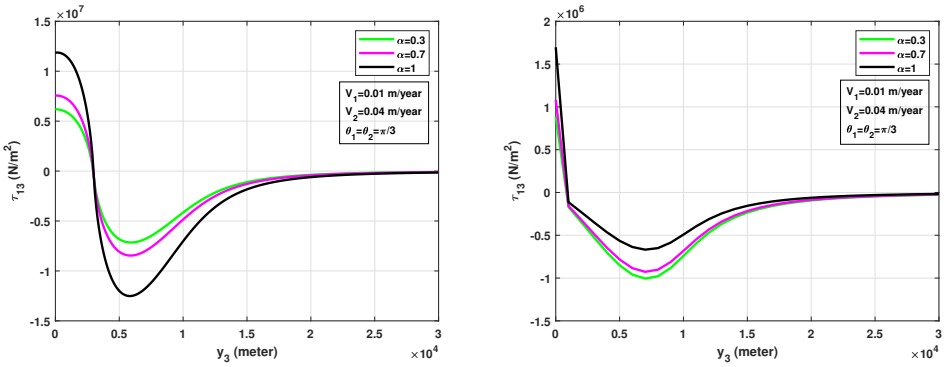
(a) (b)

Fig. 5: Driving force against time t (Case-II) for (a) different velocities V_1 across F_1, (b) different velocities V_2 across F_2.

figure 5a. The accumulated or released driving force observed in this study is of the order of 10^6, consistent with the trends reported by Kundu and Sarkar (Mondal), 2020, although differing in magnitude. The relatively lower values obtained here may be a consequence of incorporating a fractional viscoelastic model in the analysis.

Change of shear stress τ_{13} due to movement of both faults:

Figure 6a shows the changes in surface shear stress τ_{13} against y_3 for different α when both the faults are infinite (case-I), while figure 6b shows that of when first fault is infinite and the second is finite (case-II). In both cases, we are taking $V_1 = 0.01$



(a) (b)

Fig. 6: Shear stress τ_{13} against y_3 for the different orders of the fractional derivatives for (a) Case-I, (b) Case-II.

m/year and $V_2 = 0.04$ m/year and $\theta_1 = \theta_2 = \pi/3$. We observed that the accumulation/release of shear stress is significantly higher for Case-I, compared to the Case-II. For both cases, the accumulation and release of shear stress are highest in magnitude when $\alpha = 0.3$ and lowest when $\alpha = 1$. This behavior can be attributed to the slower stress relaxation at lower values of α, which reflects the longer "memory" of the system. As $y_3 \to \infty$, shear stress τ_{13} tends to zero for all cases.

It is evident that changes in surface shear stress τ_{13} is strongly depend on the fractional order derivative α for both cases and is lies in the range of 10^7 and 10^6, respectively. This outcome aligns with the results reported by Rafie et al. (2023), further supporting the credibility of the fractional model and its ability to capture the observed variations in stress.

Regions of stress accumulation and reduction:

Figure 7 presents a contour map illustrating the spatial distribution of the shear stress component τ_{12} due to the dislocation of the first fault only. The color gradient shown alongside the figure represents the magnitude of τ_{12} in units of N/m^2, with different colors denoting varying levels of stress. Positive values of τ_{12} correspond to regions of stress accumulation, while negative values indicate regions of stress reduction or release.

The contours clearly demonstrate that the most significant variations in shear stress occur in close proximity to the fault dislocation. Adjacent to the free surface, there is a noticeable accumulation of shear stress. This is likely due to the constraint imposed by the free surface boundary conditions, which prevent the material from fully relaxing the stress introduced by fault movement.

In contrast, the highest release of shear stress is observed at depths ranging from approximately 1000 m (where the fault lies) to 6818 m (approximately) below the free surface. This suggests that fault dislocation leads to a substantial redistribution

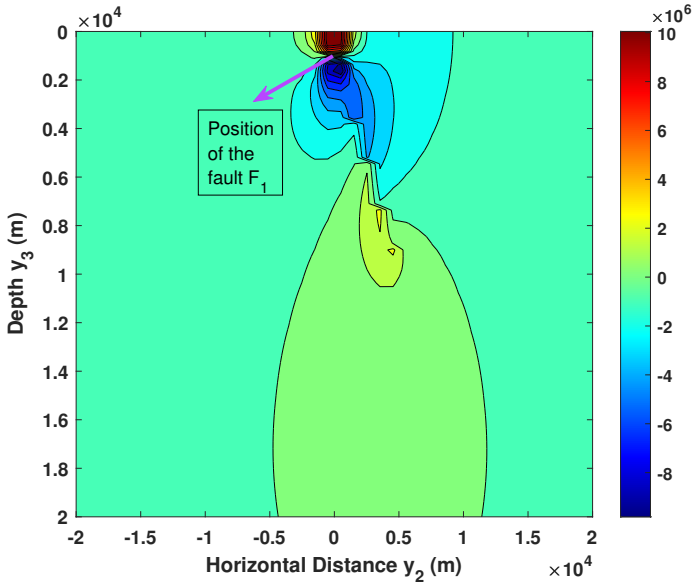


Fig. 7: Stress (τ_{12}) accumulation and reduction regions due to dislocation of the first fault only.

of shear stress along the width of the fault. Below 6818 m (approx.) depth, the accumulation or release of stress is almost negligible, indicating that the impact of the fault dislocation diminishes with depth below the free surface. This pattern is consistent with the decay of stress perturbations away from the fault zone, as the influence of the dislocation becomes less significant at greater distances.

Figure 8 displays a contour map illustrating the spatial distribution of the shear stress component τ_{12} resulting from the dislocation of two faults, each assumed to be infinitely long. The faults are situated at depths of 1 km and 3 km below the free surface, with a horizontal separation of 8 km between the upper edges of the two faults (as mentioned below "Numerical Computation").

The contour plot reveals distinct regions of stress accumulation and reduction. Notably, significant stress reduction is observed in the vicinity of both faults, with the most prominent changes occurring near the second (deeper) fault. This stress reduction diminishes progressively with increasing depth, indicating that the influence of the fault dislocations becomes less pronounced farther from the fault planes.

In the upper portion of the domain, particularly near the locations of the fault dislocations, the distribution of shear stress τ_{12} is asymmetric. The stress field exhibits a higher intensity on the right-hand side of the faults, especially for the upper fault, suggesting that the right side of each fault is undergoing more substantial displacement or movement.

As one moves deeper below the surface, the influence of the fault dislocations extends more symmetrically across both sides of the faults, reflecting the natural

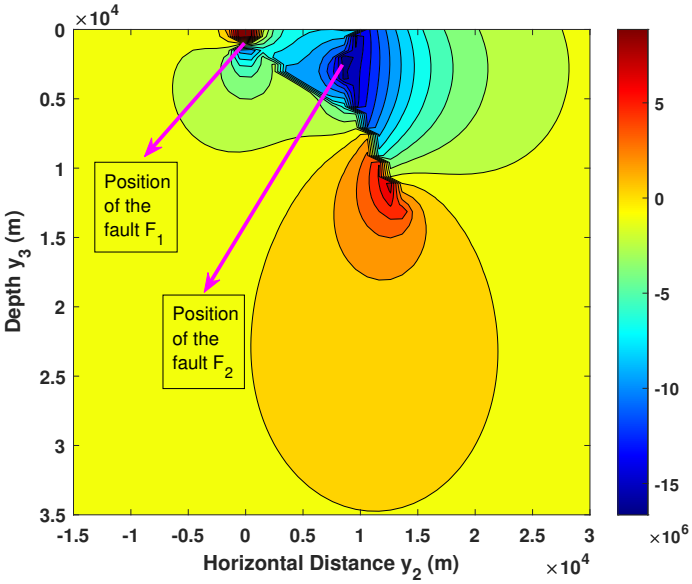
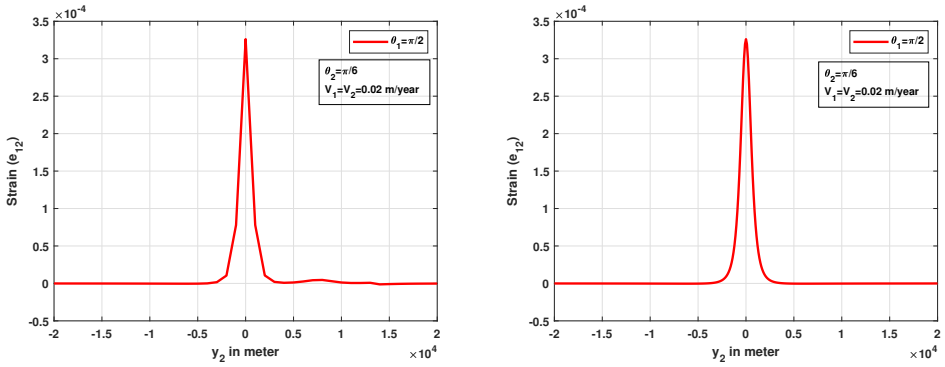


Fig. 8: Stress (τ_{12}) accumulation and reduction regions due to dislocation of both the faults (both the faults are infinite).

diffusion of stress through the surrounding medium. However, the overall magnitude of stress variations decreases with depth, consistent with the attenuation of stress disturbances farther from their origin.

Change of strain on the free surface:
Figure 9a analyze the variation of shear strain e_{12} against y_2 for $\theta_1 = \frac{\pi}{2}$, under the condition that both faults F_1 and F_2 are considered infinite in extent. In contrast, Figure 9b presents a similar analysis where the first fault F_1 is infinite, but the second fault F_2 is finite in length. In both scenarios, a pronounced release of shear strain is observed very close to the fault plane, specifically near $y_2 = 0$, which corresponds to the location of the primary fault F_1. The peak strain release occurs precisely at this point, indicating that the highest shear deformation is concentrated along the fault trace. As $|y_2|$ increases, the magnitude of shear strain release gradually diminishes for all values of θ_1.

The computed shear strain e_{12} is found to vary in the range of approximately 10^{-4}, which aligns well with observed geophysical data. For instance, studies of real-world strike-slip faulting, such as during the 2011 Tohoku-oki earthquake, have documented shear strain changes in the range of 10^{-4} to 10^{-7} (Takagi and Okubo, 2017). Thus, the numerical results presented in Figures 9a and 9b are consistent with observed strain behavior in natural fault systems, reinforcing the validity of the adopted modeling approach.



(a) (b)

Fig. 9: Changes of strain e_{12} against y_2 for (a) Case-I, (b) Case-II.

5 Conclusion

Here, we have observed the ground deformation due to the (i) interaction of two infinite buried faults (figure 1a), and (ii) interaction of one infinite buried and another finite surface-breaking fault (figure 1b), during the aseismic period in a fractional standard linear solid medium. To formulate the model as general as possible, the order of the fractional derivative is considered in the interval $(0, 1]$ to determine displacements, stresses, and strains.

We observe from numerical results that when both the faults creep, the change in displacement is of the order of 10^{-3} near both the faults (figure 3). For case-I (figure 3a), this change near the second fault is higher in magnitude than that of the first fault, while for case II (figure 3b), this change near the second fault is lower in magnitude than that near the other. For both cases, as we move away from the first fault, the rate of displacement decreases on either side of it, but as we move further towards the second fault from the first, an increase in the rate of displacement is clearly observed.

Some interesting features were also observed from the figures of the driving force (figure 4, 5). When both faults creep, there is a rapid release of stress with varying rates for different inclinations and various creep velocities of the first fault.

As the value of α increases, the rate of release of stress also increases (figure 6). Hence, we conclude that the rate of release of stress depends on the inclinations and creep velocities of both faults, as well as on the value of the order of the fractional derivative. The different values of α $(0 < \alpha \leq 1)$ exhibit that the analytic model developed in our work demonstrates increased elasticity and enhanced memory effects. This is why our model may be considered to be more general in representing the physical phenomena of fault interaction. The contour map of figure 8 suggests that the interaction of two infinite faults influences the stress field more extensively

than a single fault.

The graphical results derived from our fractional model show strong agreement with observed geophysical data, as detailed in the corresponding sections. In comparison to the integer-order model developed by Kundu and Sarkar (Mondal) (2020), our approach offers noticeably greater accuracy in capturing the complexities of real-world deformation patterns. This indicates that the fractional model serves as a more precise tool for predicting seismic behavior than traditional integer-order formulations.

6 Future Scope

It is observed that earthquakes occur due to the interaction of the faults that are dip-slip/locked in nature (San Andreas fault). Our model can be extended to analyze the interaction of such faults for displacement, stresses, and strains. Moreover, there is scope to consider the medium as a viscoelastic half-space following Burger's rheology or as a layered medium overlying a viscoelastic half-space, offering further insights into fault movements and their impact. Since non-planar faults can also be observed in physical phenomena, our model can be further developed to analyze the interaction of non-planar faults.

Declaration

- **Acknowledgements**
  Pabita Mahato, the first author, sincerely acknowledges the National Institute of Technology, Durgapur, India, for its essential support.

- **Ethics approval and consent to participate**
  The present research did not include experiments involving human subjects or animals.
- **Competing interests**
  The authors declare no conflict of interest.
- **Authors' contributions**
  The first author prepared the initial draft and was primarily responsible for developing and executing the code used in the study. The second author oversaw the work, contributed to manuscript revisions, and enhanced its overall clarity and language. The third author assisted in refining the manuscript further and contributed to improving its overall quality.
- **Availability of data and materials**
  This study is based on data obtained from earlier published research, with all sources properly cited within the text to acknowledge the original contributions.

References

[1] Bischoff S H, Flesch L M (2018) Normal faulting and viscous buckling in the Tibetan Plateau induced by a weak lower-crust. Nature Communications 9(1): 4952

[2] Caputo, M.: Linear models of dissipation whose Q is almost frequency independent—II. Geophysical Journal International 13(5), 529-539 (1967). https://doi.org/10.1111/j.1365-246X.1967.tb02303.x

[3] Debnath, L.: Recent applications of fractional calculus to science and engineering. International Journal of Mathematics and Mathematical Sciences 2003(54), 3413-3442 (2003). https://doi.org/10.1155/S0161171203301486

[4] Debnath, S. K., Sen, S.: Two interacting creeping vertical rectangular strike-slip faults in a viscoelastic half-space model of the lithosphere. International Journal of Scientific and Engineering Research 4, 1058-1071 (2013)

[5] Debnath, P., Sen, S.: Two neighboring strike-slip faults and their interaction. IOSR Journal of Applied Geology and Geophysics 2, 44-56 (2014). https://doi.org/10.9790/0990-02614456

[6] Deng, W., Morozov, I. B.: Mechanical interpretation and generalization of the Cole-Cole model in viscoelasticity. Geophysics 83(6), MR345-MR352 (2018)

[7] Ge, W., Shen, Z., Molnar, P., Wang, M., Zhang, P., Yuan, D.: GPS determined asymmetric deformation across central Altyn Tagh fault reveals rheological structure of northern Tibet. J. Geophys. Res. Solid Earth 127(9), e2022JB024216 (2022). https://doi.org/10.1029/2022JB024216

[8] Ghosh, U., Mukhopadhyay, A., Sen, S.: On two interacting creeping vertical surface-breaking strike-slip faults in a two-layer model of the lithosphere. Physics of the earth and planetary interiors 70(1-2), 119-129 (1992). https://doi.org/10.1016/0031-9201(92)90166-S

[9] Harris, R. A., Day, S. M.: Dynamics of fault interaction: Parallel strike-slip faults. Journal of Geophysical Research: Solid Earth 98(B3), 4461-4472 (1993). https://doi.org/10.1029/92JB02272

[10] Hilfer, R. Ed.: Applications of fractional calculus in physics. World scientific (2000). https://doi.org/10.1142/3779

[11] Kato, N., Lei, X.: Interaction of parallel strike-slip faults and a characteristic distance in the spatial distribution of active faults. Geophysical Journal International 144(1), 157-164 (2001). https://doi.org/10.1046/j.0956-540X.2000.01310.x

[12] Kundu, P., Sarkar (Mondal), S.: Deformation analysis of a viscoelastic half-space due to a finite and an infinite interacting faults. Physica Scripta 95(5), 055004 (2020). https://doi.org/10.1088/1402-4896/ab6f94

[13] Kundu, P.: Analysis of ground deformation due to movement of a sequence of interacting fault model. Modeling Earth Systems and Environment 10(2), 2733-2748 (2024). https://doi.org/10.1007/s40808-023-01922-z

[14] Mahato, P., Mondal, D., Sarkar (Mondal), S.: Determination of effect of the movement of an infinite fault in viscoelastic half space of standard linear solid using fractional calculus. Physica Scripta 97(12), 125015 (2022). https://doi.org/10.1088/1402-4896/ac9caa

[15] Mahato, P., Sarkar Mondal, S.: Effect on surface deformation due to interacting fault in fractional standard linear solid. GEM-International Journal on Geomathematics 16(1), 5 (2025).https://doi.org/10.1007/s13137-025-00264-5

[16] Maji, M., Sen, S., Pal, B. P., Mukhopadhyay, A.: On stress accumulation in the lithosphere and interaction between two strike-slip faults. Mausam 30(2, 3), 359-363 (1979). https://doi.org/10.54302/mausam.v30i2.3056

[17] Manna, K., Sen, S.: Interacting inclined strike-slip faults in a layered medium. Mausam 68(3), 487-498 (2017). https://doi.org/10.54302/mausam.v68i3.701

[18] Maruyama, T: On Two-Dimensional Elastic Dislocations in an Infinite and Semi-infinite Medium. Bulletin of the Earthquake Research Institute 44(1), 811-871 (1966)

[19] Mittag-Leffler, G.M.: Sur la nouvelle fonction $E_\alpha(x)$. CR Acad Sci Paris 137(2), 554-558 (1903)

[20] Mondal, D., Kundu, P., Sarkar (Mondal), S.: Accumulation of Stress and Strain due to an Infinite Strike-Slip Fault in an Elastic Layer Overlying a Viscoelastic Half Space of Standard Linear Solid (SLS). Pure and Applied Geophysics 177(10) 4643-4656 (2020). https://doi.org/10.1007/s00024-020-02536-7

[21] Mondal, D., Debnath, P.: An application of fractional calculus to geophysics: effect of a strike-slip fault on displacement, stresses and strains in a fractional order Maxwell type viscoelastic half space. International Journal of Applied Mathematics 34(5), 873 (2021). https://doi.org/10.12732/ijam.v34i5.2

[22] Özalp, N., Demirci, E.: A fractional order SEIR model with vertical transmission. Mathematical and Computer Modelling 54(1-2) 1-6 (2011). https://doi.org/10.1016/j.mcm.2010.12.051

[23] Parsons, T., Sliter, R., Geist, E.L., Jachens, R.C., Jaffe, B.E., Foxgrover, A., Hart, P.E. and McCarthy, J.: Structure and mechanics of the Hayward–Rodgers

Creek fault step-over San Francisco Bay, California. Bulletin of the Seismological Society of America 93(5), 2187-2200 (2003). https://doi.org/10.1785/0120020228

[24] Pelap, F.B., Tanekou, G.B., Fogang, C.F., Kengne, R.: Fractional-order stability analysis of earthquake dynamics. Journal of Geophysics and Engineering 15(4), 1673-1687. https://doi.org/10.1088/1742-2140/aabe61

[25] Petersen, M.D.: Probabilistic seismic hazard assessment for the state of California. California Department of Conservation Division of Mines and Geology 96(8) (1996)

[26] Podlubny, I.: Fractional differential equations. san diego ca: Academic (1999)

[27] Rafie, M.T., Sahara, D.P., Cummins, P.R., Triyoso, W., Widiyantoro, S.: Stress accumulation and earthquake activity on the Great Sumatran Fault, Indonesia. Natural Hazards 116(3), 3401-3425 (2023). https://doi.org/10.1007/s11069-023-05816-2

[28] Rybicki, K.: The elastic residual field of a very long strike-slip fault in the presence of a discontinuity, Bull. Seismol. Soc. Am. 61(1), 79-92 (1971)

[29] Samko, S.G., Kilbas, A.A., Marichev, O.I.: Fractional Integrals and Derivatives: Theory and Applications, New York CRC (1993)

[30] Segall, P.: Earthquake and volcano deformation. Princeton University Press (2010)

[31] Shao, B., Hou, G.: The interactions of fault patterns and stress fields during active faulting in Central North China Block: Insights from numerical simulations. Plos one 14(4), e0215893 (2019). https://doi.org/10.1371/journal.pone.0215893

[32] Takagi, Y., Okubo, S.: Internal deformation caused by a point dislocation in a uniform elastic sphere. Geophysical Journal International 208(2), 973-991 (2017). https://doi.org/10.1093/gji/ggw424

[33] Titus, S.J., DeMets, C., Tikoff, B.: Thirty-five-year creep rates for the creeping segment of the San Andreas fault and the effects of the 2004 Parkfield earthquake: constraints from alignment arrays, continuous global positioning system, and creepmeters. Bulletin of the Seismological Society of America 96(4B), S250–S268 (2006). https://doi.org/10.1785/0120050811

[34] Turcotte, D.L., Gerald, S.: Geodynamics. Cambridge University Press, Cambridge (2002)

[35] Wu, F., Ji, C., Liu, J., Gao, R., Li, C., Zou, Q., Chen, J.: Study on visco-elastoplastic fractional creep model of surrounding rock of salt cavern gas storage. Journal of Energy Storage 67, 107606 (2023).